

Contribution of multiple electron trajectories to high-harmonic generation in the few-cycle regimeA. Yu. Naumov,¹ D. M. Villeneuve,¹ and Hiromichi Niikura^{1,2,3,*}¹*National Research Council of Canada, 100 Sussex Drive, Ottawa, Ontario, Canada K1A 0R6*²*Department of Applied Physics, Waseda University, Okubo 3-4-1, Shinjyuku, Tokyo 169-8555, Japan*³*PRESTO, Japan Science and Technology Agency, 4-1-8 Honcho Kawaguchi, Saitama 332-0012, Japan*

(Received 7 May 2015; published 26 June 2015)

We use a few-cycle, carrier-envelope-phase (CEP) stabilized laser system to generate high-harmonic emission in argon, neon, and carbon dioxide. The high-harmonic spectra consist of discrete harmonic orders whose positions shift as a function of the CEP. Near the cutoff harmonic, the peaks are separated by two photon orders, and can correspond to either even or odd harmonics of the driving laser frequency, depending on the value of the CEP. In the plateau region, harmonic orders are separated by only one photon order. We develop a simple model which predicts the observed behavior. We use the observed dependence of the harmonic peaks as a function of CEP as a method to measure the statistical CEP fluctuations of the laser system. The measured rms fluctuation of 0.17 radians agrees with optical measurements. The high-harmonic approach to measuring CEP stability has the advantage that it is less sensitive to laser intensity fluctuations than are optical methods.

DOI: [10.1103/PhysRevA.91.063421](https://doi.org/10.1103/PhysRevA.91.063421)

PACS number(s): 33.20.Xx, 42.65.Re

I. INTRODUCTION

High-harmonic generation was first seen as the emission spectrum composed of a series of odd multiples of the fundamental laser frequency. As laser pulse durations became shorter, it was realized that the rule of strict odd harmonic orders was not obeyed. Here we will record experimentally the positions of the harmonic orders produced by intense few-cycle laser pulses as the carrier-envelope-phase of the laser is varied. Using a simple model, we will attribute the positions of the various orders to spectral interference between adjacent attosecond pulses.

High-harmonic generation [1–3] is used as a probe to observe attosecond dynamics in atoms and molecules [4]. The amplitude, phase, and polarization of a high-harmonic spectrum include information on electronic [5–8] and structural dynamics of molecules [9,10] from which the harmonics are emitted. The attosecond electron dynamics can be mapped onto a continuum harmonic spectrum in a single, isolated attosecond pulse [11]. The high harmonics are generated by the interaction between gas-phase atoms or molecules and an intense driving laser pulse. Based on the three-step model [12], at every half optical cycle of the driving laser pulse, part of the bound electronic wave function is released to the ionization continuum by tunnel ionization. The electron is accelerated by the laser field and recollides with the parent ion within one optical cycle after tunnel ionization, leading to a single attosecond emission [1]. Since this three-step process occurs twice during every optical cycle, a train of single attosecond pulses is generated in a multiple-cycle, linearly polarized driving laser pulse. In the long pulse limit, each attosecond pulse has the same amplitude, and there is a one-to-one mapping between the emitted photon energy and the emission time, when only the short trajectory is selected [11,13]. However, for laser pulses that are only a few optical cycles in duration, the phase and amplitude of the attosecond pulses depend on the instantaneous intensity and the carrier-envelope

phase (CEP) of the driving laser field [14–17], which makes the high-harmonic spectrum more complicated.

In this work we study, theoretically and experimentally, the CEP dependence of the high-harmonic spectra generated from atoms and molecules in the few-cycle pulse regime. Using a linearly or a time-dependent polarized CEP-stabilized few-cycle pulse, we measure the CEP dependence of the high-harmonic spectra in CO₂, neon, and argon gases. To analyze the observed spectra, we simulate the high-harmonic spectra as a function of CEP values using the strong-field approximation (SFA) [18]. By comparing the observed spectra with the calculated spectra, the following information can be obtained: (a) the number of single attosecond emissions that contribute to the total high-harmonic spectrum in a given harmonic range, and (b) the phase difference between the adjacent single attosecond pulses. We confirm that the characteristic peak separation observed in the middle range of the high-harmonic spectra from CO₂ can be accounted for by the interaction between the three attosecond pulses, without considering other effects such as dynamical interference, chirp of the driving laser pulse, or the propagation (phase matching) effects. For neon and argon, we employ a time-dependent polarized pulse technique [15,17] to reduce the number of attosecond pulses while keeping the same driving laser pulse duration. We demonstrate that the spectral features of CO₂ and neon can be simulated by using a suitable pulse duration.

II. EXPERIMENTAL SETUP

Figure 1 illustrates the experimental setup. We generate CEP-stabilized laser pulses from a multipass Ti:sapphire amplifier (single-stage Dragon system from KMLabs, 800 nm, 1 kHz, 35 fs). The Ti:sapphire crystal is cooled down to 45 K with a specially designed vibration-isolated cryocell system. The typical output pulse energy is about 1.85 mJ per pulse. The CEP of the oscillator laser pulse is measured with an f -to- $2f$ interferometer (Menlo Systems, XPS-800) and stabilized by adjusting the length of the cavity in the Ti:sapphire oscillator with a feedback loop. We measure the CEP value of the amplified pulses with a single-shot f -to- $2f$

*Corresponding author: niikura@waseda.jp

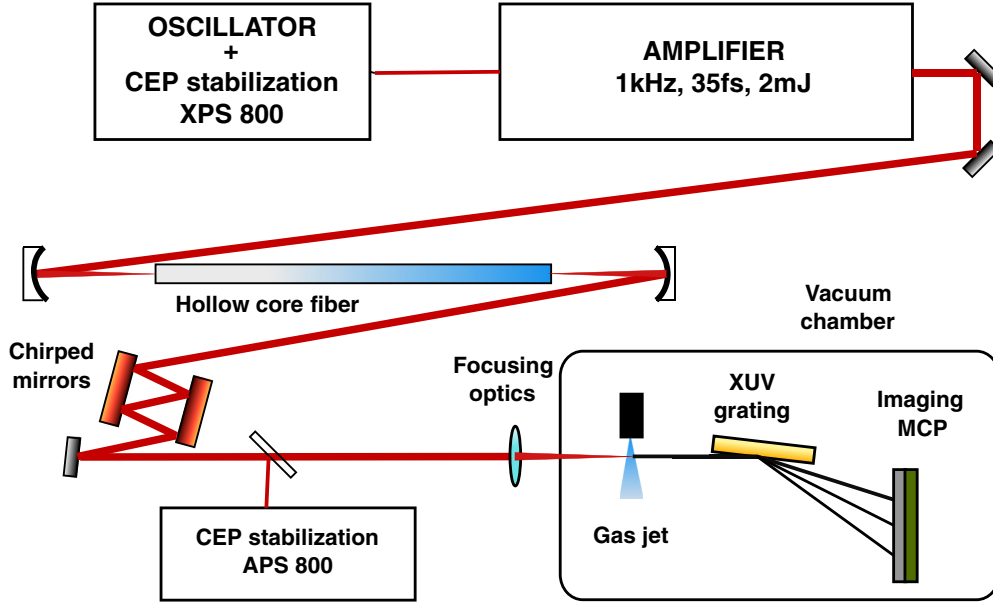


FIG. 1. (Color online) Schematic diagram of the experimental setup. A KMLabs Dragon femtosecond laser system is employed. The carrier-envelope-phase stabilized amplified laser pulses are passed through an argon gas filled hollow-core fiber of $250\ \mu\text{m}$ inside diameter to broaden the spectrum. The pulses are then compressed by a set of chirped mirrors to a duration of about 5 fs. The CEP is measured after the pulse compression using a Menlo Systems APS 800. The compressed pulses are focused into a pulsed gas jet inside a vacuum chamber to generate the high-harmonic emission that is detected with an XUV spectrometer.

interferometer (Menlo Systems, APS-800). To compensate for the slow CEP drift during the amplification process, we adjust the grating separation in the pulse compressor with a piezoelectric device [17]. The output pulse is compressed to about 5 fs by using a hollow-core fiber compressor and a set of chirped mirrors [19]. We use a 1-m-long hollow-core glass capillary with $250\ \mu\text{m}$ inner diameter, filled with argon gas to broaden the pulse spectrum by self-phase modulation. A pressure gradient with low pressure at the input end and high pressure at the output end is employed to avoid ionization of the gas at the entrance of the capillary. We compensate the group velocity dispersion of the laser pulse with a set of chirped mirrors (Femtolasers GSM014) to reduce the pulse duration down to about 5 fs. The pulse duration is measured with a homebuilt SPIDER [20]. For the experiments in which polarization gating was employed, a crystalline quartz plate with a thickness of 0.2 mm and a quarter-wave plate were inserted into the beam path [15].

The laser beam is focused with a 500 mm focal length spherical mirror into a vacuum chamber. Harmonics are generated in a pulsed gas jet that is placed slightly before the laser focus. The length of the gas in the direction of laser propagation was about 0.5 mm, and the agreement with single-atom high-harmonics-generation (HHG) calculations confirms that good phase matching was achieved [21]. In order to capture the harmonic spectrum generated by a single driving laser pulse from the 1 kHz laser pulse train, we reduce the repetition rate of the pulsed gas jet down to 50 Hz and as low as 10 Hz for some experiments. The high-harmonic emission is spectrally dispersed by a flat-field XUV grating spectrometer (Hitachi, model 001-226). The dispersed spectrum is detected by an imaging microchannel plate (BURLE MCP) and captured by a CCD camera. We

integrate the harmonics emission in the direction perpendicular to the dispersion axis to generate the high-harmonic spectrum.

III. EXPERIMENTAL RESULTS

Figure 2(a) shows the measured high-harmonic spectra of CO_2 as a function of CEP values generated by a linearly polarized pulse with peak intensity $3.0 \times 10^{14}\ \text{W}/\text{cm}^2$ and pulse duration of ~ 5.5 fs. The CEP is varied in the $-\pi$ to π range in 0.17π increments using the APS 800 software control. We accumulate 20 spectra for each CEP value. For harmonic orders below 21, the position of the harmonics is almost independent of the CEP, while the spectral intensity modulates slightly as the CEP changes. For harmonic orders 21–27, the adjacent harmonics are separated by approximately one photon order of the driving laser field, ~ 1.55 eV, instead of the usual two photons for odd harmonics. For harmonic orders greater than 31, the adjacent harmonic peaks are separated by two photons. A similar one-photon separation in the middle range of the spectrum is also observed in the CEP-dependent high-harmonic spectrum of N_2 (not shown).

Figure 2(b) shows the CEP dependence of the high-harmonic spectra in neon gas generated by a polarization-gated pulse. The harmonic peaks shift as a function of CEP values and the spectral intensity modulates with a π period of the CEP value significantly more than that of CO_2 . This modulation period is due to the fact that the amplitude of the driving electric field is repeated with this period. The observed spectrum of neon is similar to the photoelectron spectrum reported in Ref. [22]. In our case, the spectrum is confined in the range from harmonic order 35 (~ 55 eV) to harmonic order 51 (~ 80 eV), though the spectrum is measured without a spectral filter. The adjacent harmonic peaks are separated by

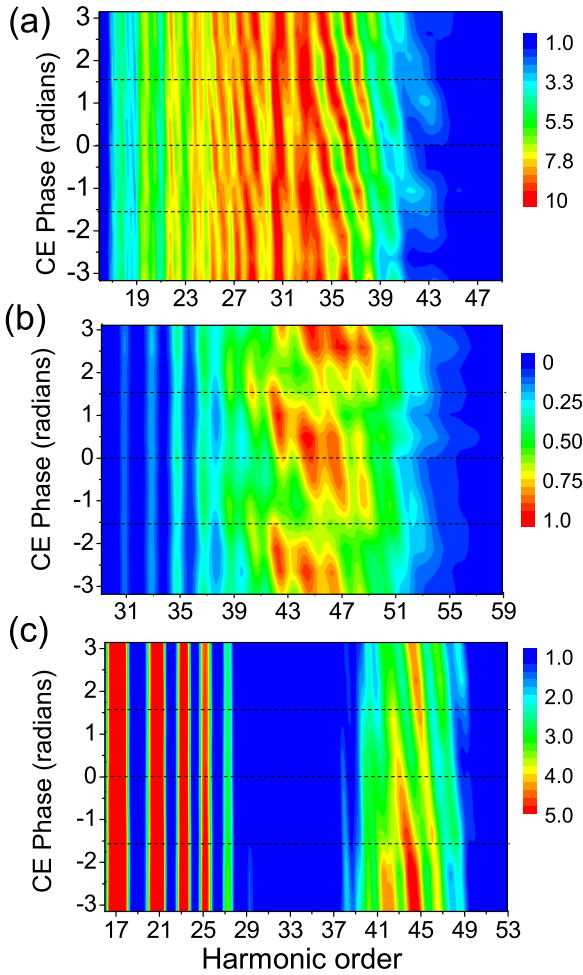


FIG. 2. (Color online) The experimentally measured high-harmonic spectra as a function of the carrier-envelope phase of the driving laser field for three different gases. (a) CO₂ gas and a linearly polarized pulse with a duration of 5.5 fs and an intensity of 3.0×10^{14} W/cm². (b) Ne gas and polarization gating to reduce the pulse duration below 5 fs. (c) Ar gas and the same polarization gating technique as in (b).

approximately two harmonic orders. Like in the case of CO₂, the position of the low harmonics is not affected by the CEP.

Figure 2(c) shows the CEP dependence of the high-harmonic spectra in argon produced using the same time-dependent polarization pulse as in neon. As has been reported in Ref. [21], the intensity of the harmonics is minimized around 51 eV. The photon energy of the harmonic peaks observed below harmonic 29 is independent of the CEP value, while in the range from harmonic 41 to 49, the photon energy of the harmonic peaks shifts as a function of CEP and the intensity is slightly modulated.

We now want to investigate why the positions of the harmonic orders are affected by the CEP. For a long laser pulse, with many optical cycles, by symmetry the harmonic orders must correspond to odd multiples of the laser frequency [23]. When the laser pulse is composed of only a few optical cycles, this symmetry breaks down. The position of the harmonic orders can then differ from exactly odd harmonics of the laser

frequency, and can depend on the exact shape of the laser pulse.

IV. SFA MODEL

We model the experimental results using a simple SFA model [18] using the implementation suggested in [24]. The laser field is described by a carrier frequency with a Gaussian envelope to give the desired full width at half maximum (FWHM) duration, i.e.,

$$E(t) = E_0 \exp[-(2 \ln 2)t^2/\tau_p^2] \cos(\omega_0 t - \phi). \quad (1)$$

Here E_0 is the peak laser electric field, t is time, τ_p is the FWHM pulse duration, ω_0 is the laser angular frequency corresponding to a wavelength of 800 nm, and ϕ is the CEP (or CE phase). It was ensured that the vector potential at the end of the pulse was zero, i.e., the integral of the electric field was zero. The peak intensity was chosen to be 2.1×10^{14} W/cm² and the ionization potential was 13.77 eV. A flat recombination dipole matrix element was used, i.e., $d(\omega) = 1$. The SFA calculation produced the electric field vs time of the XUV emission. This field was Fourier transformed to produce the high-harmonic power spectrum. The CEP was varied for each laser condition, resulting in a two-dimensional plot of the high-harmonic spectrum versus CEP.

Figure 3 shows the calculated harmonic spectra for FWHM pulse durations τ_p of (a) 11 fs, (b) 7.0 fs, (c) 5.0 fs, and (d) 3.5 fs, respectively. For $\tau_p = 11$ fs, the harmonic spectra are almost independent of the CEP value in the low and middle harmonic spectral ranges. In the cut-off region, the harmonic peaks shift slightly as a function of CEP and subpeaks appear between the odd harmonics. For $\tau_p = 7.0$ fs, the location of the harmonic peaks varies with the CEP value in both middle and cut-off ranges. In the middle spectral range the harmonic peaks are separated by approximately one harmonic order at certain CEP values, and by approximately two harmonic orders in the cut-off range. These spectral features are consistent with the observed high-harmonic spectra of CO₂ shown in Fig. 2(a). The calculations also show that for the longer pulse durations, there are additional peaks between the usual odd harmonic orders for the higher photon ranges. For the shorter pulse durations, these additional peaks disappear, leading to emission with the usual two-photon spacing. However, the positions of the peaks shift as the CEP value is varied. This behavior is consistent with that shown numerically for the case of short pulses produced by polarization gating [25], and with that shown analytically [26].

We characterize the CEP dependence of the positions of the harmonic orders around harmonic 35 by the slope $dq/d\phi$, where $q = \omega/\omega_0$ is the harmonic order and ϕ is the CEP. This slope increases for shorter pulse durations: at 11 fs there is little evidence of shifting peaks, at 7 fs it is $dq/d\phi = -1/\pi$, at 5 fs it is $dq/d\phi = -2/\pi$, and at 3.5 fs it is $dq/d\phi = -4/\pi$. The experimental results in Fig. 2 show a slope of $dq/d\phi = -2/\pi$, which corresponds to the SFA calculations for $\tau_p = 5$ fs. For the calculation at $\tau_p = 3.5$ fs, the spectral intensity of the harmonic peaks is modulated significantly as a function of CEP values, as is observed experimentally in Fig. 2(b). This modulation is mainly caused by the fact that the tunnel ionization probability depends on the CEP values.

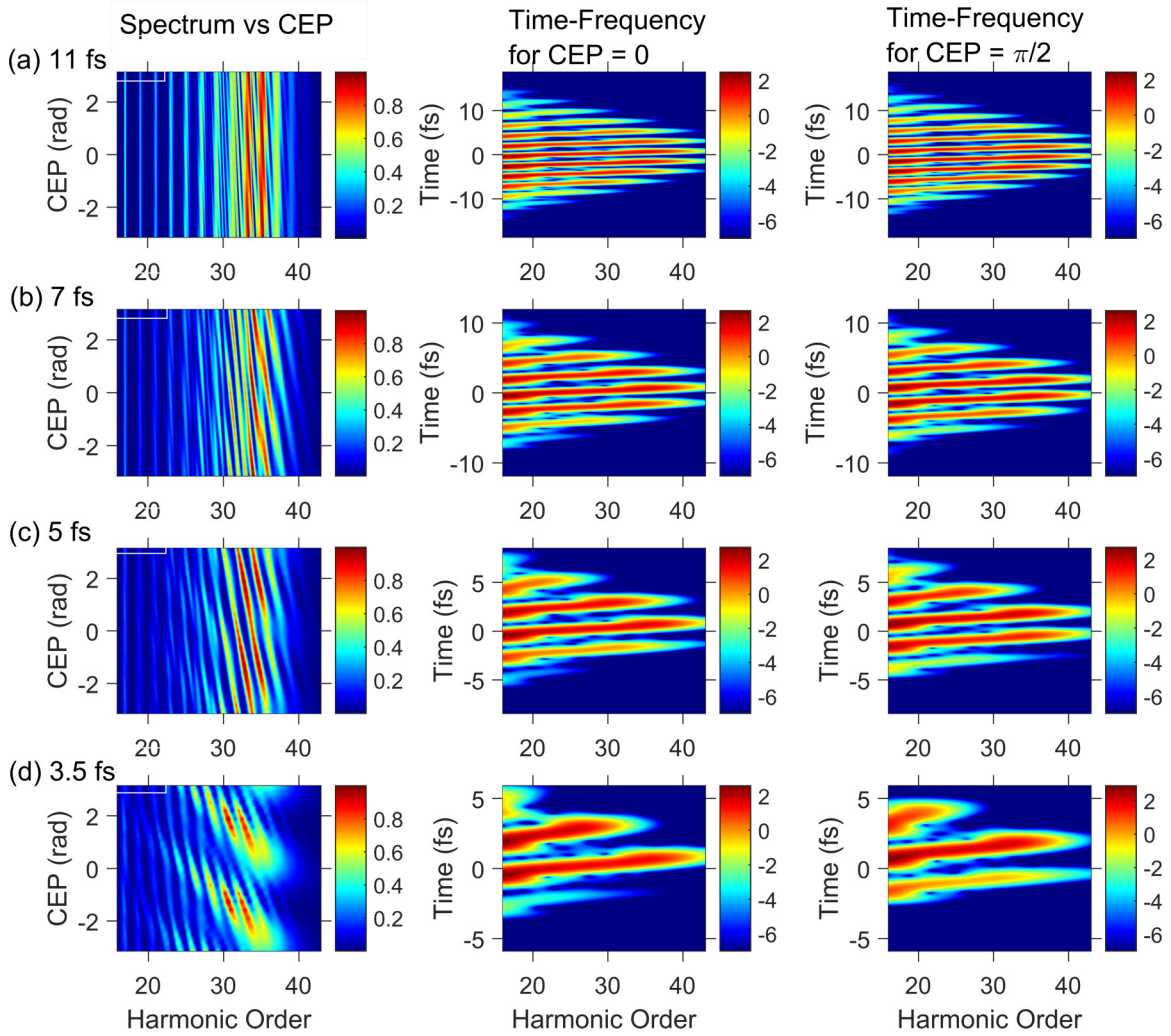


FIG. 3. (Color online) Calculated high-harmonic spectra as a function of the carrier-envelope phase of the driving laser field. The SFA model is used to calculate the spectrum at each CEP value. The peak laser intensity is $2.1 \times 10^{14} \text{ W/cm}^2$ at a wavelength of 800 nm. The recombination dipole moment is set to unity and the ionization potential is 13.77 eV. Full width at half maximum intensity (FWHM) of pulse durations are (a) 11 fs, (b) 7 fs, (c) 5 fs, and (d) 3.5 fs. The left column shows the dependence of the spectra on the CEP value. The middle column shows the time-frequency dependence for CEP = 0 (relative to a cosine field). The right column shows the time-frequency dependence for CEP = $\pi/2$.

V. ANALYTIC MODEL

To further understand the behavior predicted by the SFA calculations in Fig. 3, we illustrate the relationship between the spectral phase and the photon energy shift of the harmonic peak using a simple analytic model. Using this simple approach, we are able to qualitatively understand the CEP dependence of the spectra in Fig. 2.

We first consider the case of a very short driving laser field, where only two single attosecond emissions contribute to the total high-harmonic spectra. To make it more clear, we assume that the two attosecond pulses are identical except for a time delay and a phase shift. At a small photon energy range centered around the XUV frequency ω , the total radiating dipole moment, $D(t)$, is given by the sum of the two attosecond pulses, labeled 1 and 2, each represented by $d(t)$,

$$D(t) = d(t) + d(t - T_0)\exp[i(\pi + \theta_{12})]. \quad (2)$$

Here $T_0 = \pi/\omega_0$ is half of the optical period of the 800 nm laser field. The second pulse is delayed in time by T_0 and inverted in sign (by the π phase shift). Here θ_{12} is an additional phase difference between the two single attosecond pulses at that energy, in addition to the delay and sign inversion. The spectral amplitude, $D(\omega)$, is given by the Fourier transform of $D(t)$,

$$\begin{aligned} D(\omega) &= \int D(t) \exp(-i\omega t) dt \\ &= d(\omega) \{1 + \exp[i(\pi + \omega T_0 + \theta_{12})]\}. \end{aligned} \quad (3)$$

Here $d(\omega)$ is the Fourier transform of the single attosecond pulse represented by $d(t)$. The power spectrum is the absolute square of $D(\omega)$,

$$S(\omega) = |D(\omega)|^2 = 2|d(\omega)|^2 [1 + \cos(\pi + \omega T_0 + \theta_{12})]. \quad (4)$$

The term in square brackets modulates the spectrum of the single attosecond pulse, with peaks appearing when $\pi +$

$\omega T_0 + \theta_{12} = 2n\pi$, where n is an integer. For example, when the relative phase between the two attosecond pulses is $\theta_{12} = 0$, this relation becomes $\omega = (2n + 1)\omega_0$, i.e., odd harmonics of the driving laser frequency. When $\theta = \pi$, the relation becomes $\omega = 2n\omega_0$, i.e., even harmonics. In general, the spectral peaks occur at

$$\frac{\omega}{\omega_0} = 2n - 1 - \theta_{12}/\pi. \quad (5)$$

Thus, any additional phase difference between attosecond pulses can shift the positions of the harmonic orders in the spectrum. Here θ_{12} is actually a function of ω , and it is nonzero if the alternate half-cycles of the laser pulse are not identical. This occurs when the amplitudes of the half-cycles are different. For a short pulse, it can be seen that changing the CEP will cause the amplitudes of half-cycles to differ, and hence will lead to a shift in the high-harmonic peaks.

When three single attosecond emissions, labeled 1, 2, and 3, contribute to the total high-harmonic spectra, the total dipole moment is given by

$$D(\omega) = d(\omega)\{1 + \exp[i(\pi + \omega T_0 + \theta_{12})] + \exp[i(2\pi + 2\omega T_0 + \theta_{13})]\}, \quad (6)$$

where θ_{12} and θ_{13} are the phase differences from the phase of the first single emission. By squaring the factor in square brackets as before, and looking for what frequencies correspond to peaks in the spectrum, we find interferences between all three terms:

$$\frac{\omega}{\omega_0} = 2n - 1 - \theta_{12}/\pi, \quad (7)$$

$$\frac{\omega}{\omega_0} = n - \theta_{13}/2\pi, \quad (8)$$

$$\frac{\omega}{\omega_0} = 2n - 1 - \theta_{23}/\pi. \quad (9)$$

The two terms, Eq. (7) and Eq. (9), can correspond to either even or odd harmonics. This can cause the harmonic peaks to be separated by approximately one harmonic number as seen in Fig. 3(b). The term in Eq. (8) can be seen to be the average of Eqs. (7) and (9), and so gives a peak between the other two peaks.

This simple model illustrates the three regimes of CEP dependence observed in Figs. 2 and 3. For the lower harmonic orders which are produced even at the lowest intensity part of the pulse temporal envelope, there is no CEP dependence on the position of the peaks, because many half-cycles contribute to the emission and there is little difference between adjacent half-cycles (θ is small). In the middle part of the spectrum, only a few half-cycles contribute, resulting in a mixture of even, odd, and shifted harmonic orders. Near the cutoff, only the highest intensity part of the pulse contributes, and for a short pulse duration this means only two attosecond pulses contribute to the signal. This produces odd harmonics only, which are shifted linearly by the phase difference between them.

We now calculate the actual phases of each single attosecond pulse using a realistic laser field. In this model, we include three single attosecond pulses generated around the center of the laser pulse envelope. In the Appendix, we illustrate

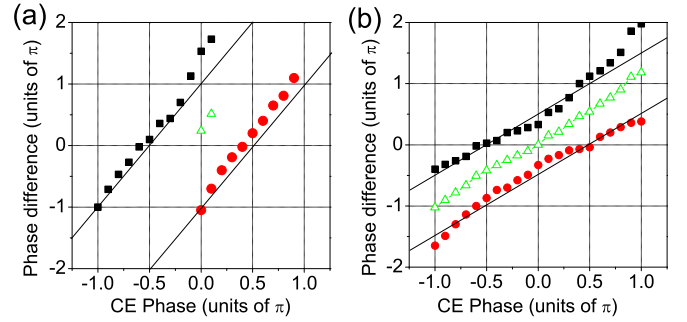


FIG. 4. (Color online) The calculated phase difference between the two adjacent single attosecond emissions in two energy regions: (a) 35th and (b) 27th harmonic order. The square (or circle) data points represent the phase difference between the first and the second single emissions, θ_{12} (or the second and the third single emissions, θ_{23}), respectively (see text). The triangle data points are plots of $\theta_{13}/2$. The solid lines are plots of the linear relationship between the CE phase and the phase difference with a slope of (a) $d\theta/d\phi = 2$ and (b) $d\theta/d\phi = 1$, respectively.

schematically the electric field of the driving laser pulse and the electron trajectories that will be considered (Fig. 8). The phase accumulated during each trajectory with canonical momentum p is the Volkov phase, calculated as

$$S(t, t', p) = \int_{t'}^t \frac{[p + A(\tau)]^2}{2} d\tau + I_p(t - t'). \quad (10)$$

This Volkov phase includes both the phase of continuum electron and the phase of the bound wave function. It does not include the emission time term, since we are only interested in differences and the emission time cancels.

Using Eq. (10), we calculate the spectral phase of three single emissions labeled as 1, 2, 3 and the phase difference between the adjacent single emissions as a function of the CEP values. Figure 4 shows the results of the calculation for the (a) 35th and (b) 27th harmonics. The circle (or square) data points in Fig. 4 show the phase difference between the first and second attosecond emissions, referred to as θ_{12} (or the difference between the second and third single emissions, θ_{23}), respectively. For Fig. 4(a), since only two single attosecond emissions contribute to the total harmonic emission except for the small range around CEP of zero (see also Fig. 10 in the Appendix), only a single phase difference, either θ_{12} or θ_{23} , contributes to the harmonic peak in the spectrum. On the other hand, for Fig. 4(b), since three trajectories contribute to the total harmonic emission, both phase difference terms θ_{12} and θ_{23} lead to the harmonic peaks in the spectra which are separated by one harmonic order. In Fig. 4, we also plot the phase difference between the first and third single emissions, $\theta_{13}/2$, as triangle data points for each harmonic order.

Next, we focus on the slope $dq/d\phi$, i.e., how quickly the harmonic peaks shift as the CEP is varied. We need two pieces of information to do this—the dependence of the CEP on the Volkov phase S [Eq. (10)], and the dependence of the predicted peak frequencies on the attosecond pulse phase differences θ_{12} , etc. [Eqs. (5) and (7)–(9)]. Figure 4 determines the slope $d\theta_{12}/d\phi$, and Eqs. (5) and (7)–(9) determine the slope

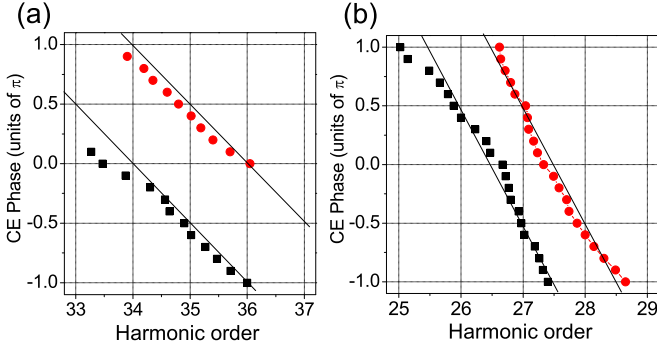


FIG. 5. (Color online) The simple analytic model presented in the text predicts the position of the harmonic orders as a function of the CEP. Here the harmonic order positions are derived from the phase differences between adjacent attosecond pulses θ_{12} (square) and θ_{23} (circle), for (a) 35th and (b) 27th harmonic orders, respectively. As a reference, we plot the solid line with a slope of $dq/d\phi = -2/\pi$ for (a), and with a slope of $dq/d\phi = -1/\pi$ for (b).

$dq/d\theta_{12}$. The product of these two slopes gives us the desired $dq/d\phi$. The square (or circle) data points in Fig. 5 show the CEP as a function of the harmonic order, converted from θ_{12} (or θ_{23}) for (a) 35th and (b) 27th harmonic order, respectively. As expected, for the 35th order, the two peaks are separated by approximately two harmonic orders, while for the 27th order, they are separated by approximately one harmonic order. For reference, we plot the solid line in Fig. 5 with a slope of $dq/d\phi = -2/\pi$ for (a), and with a slope of $dq/d\phi = -1/\pi$ for (b), respectively. The calculated data points deviate slightly from a linear slope. In fact, the slope varies with the harmonic order and it becomes steeper as the harmonic order increases. The details of the calculation are described in the Appendix.

VI. MEASUREMENT OF CEP USING HIGH-HARMONICS SPECTRA

We have shown above that the positions of the high-harmonic peaks shift as the laser pulse CEP value is varied. We now show that we can use this relationship to measure the CEP value of each laser pulse. Stability of CEP in the driving laser pulse is crucial for attosecond pulse generation and measurements [1,4]. The CEP value has been measured with methods such as single-shot f -to- $2f$ interferometry [14] or stereo above-threshold ionization [27]. In this study, we use the CEP-dependent harmonic spectra to estimate the CEP stability of the driving laser pulse. We reduce the repetition rate of the HHG so that the CCD camera can record single-shot HHG spectra. To do this, we employ a pulsed gas jet whose pulse duration is shorter than the 1 ms period of the laser pulses [28], so that harmonics are produced by only a single laser pulse. The pulsed valve repetition rate is set to 10 Hz, slow enough to read out each spectrum with the CCD camera.

Figure 6 shows the observed photon energy of the harmonic peaks as a function of the CEP values in two regions of the spectra. The data points are taken from Fig. 2(a). The data deviates slightly from a linear relationship between the photon energy and the CEP value, which is seen in the calculated spectra in Figs. 3(b) and 5 as well. It is clearly visible that the two adjacent harmonic peaks are separated by two harmonic

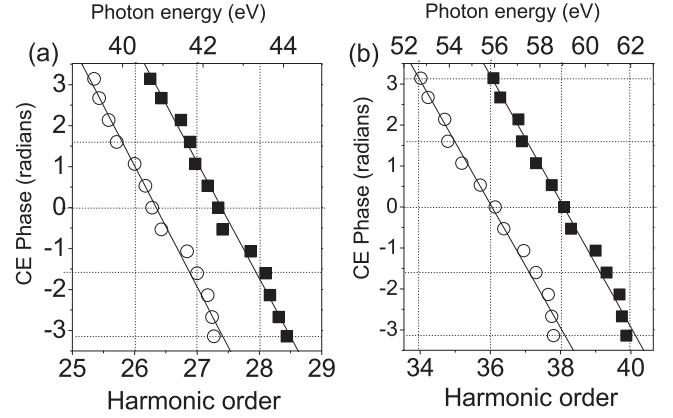


FIG. 6. The position of the experimentally observed high-harmonic peaks (circle and square data points) as a function of the value of CEP in the (a) plateau and (b) cut-off range of high-harmonic spectra of CO₂. The data points are obtained from the individual spectra shown in Fig. 2(a). The CEP causes the location of the peaks to shift. The straight lines are a least-squares fit to the data. The positions of the peaks are quite insensitive to the laser intensity; according to an SFA calculation a $\pm 10\%$ change in the laser intensity changes the position by 0.09ω in both regions.

orders in the cut-off region but by only one harmonic order in the middle range of the spectrum. The slope in the cut-off region is 0.46 radians per harmonic order. The positions of the peaks are quite insensitive to the laser intensity; according to an SFA calculation, a $\pm 10\%$ change in the laser intensity changes the peak position by 0.09ω in both regions; this is much smaller than the size of the symbols shown in Fig. 6.

Using this relationship between CEP value and the shift of the harmonic peak, we can estimate the single-shot CEP stability of the driving laser pulses. We fit the data points using a linear least-squares method. Using the slope, we convert the observed photon energy peak to CEP values. Figure 7(a) shows the high-harmonic spectra of CO₂ measured for each single laser shot while the APS 800 software stabilized the CEP value. The intensity of the spectra is represented by color coding. Figure 7(b) shows the spectrum for one of the laser shots. In Fig. 7(c), we plot the CEP value converted from the observed harmonic spectra for each laser shot. Figure 7(d) shows the distribution of CEP values over the measured single-shot spectra. The root mean square of the CEP deviation is 0.17 radian. This value is slightly smaller than that measured by our single-shot, f -to- $2f$ optical interferometer, which is 0.19 radian.

VII. CONCLUSION

In summary, we have demonstrated that the CEP dependence of the high-harmonic spectra in CO₂, neon, and argon can be analyzed by simple SFA calculations. We have confirmed that the physical origin of the extra peaks that appear in the middle range of the CO₂ spectrum can be explained by the spectral interference between three individual attosecond pulses. Finally, we conjecture that the CEP dependence of the harmonic spectra can possibly be sensitive to a spectral phase jump at a certain energy which may occur in the recombination process, e.g., the Cooper minimum in argon, because the

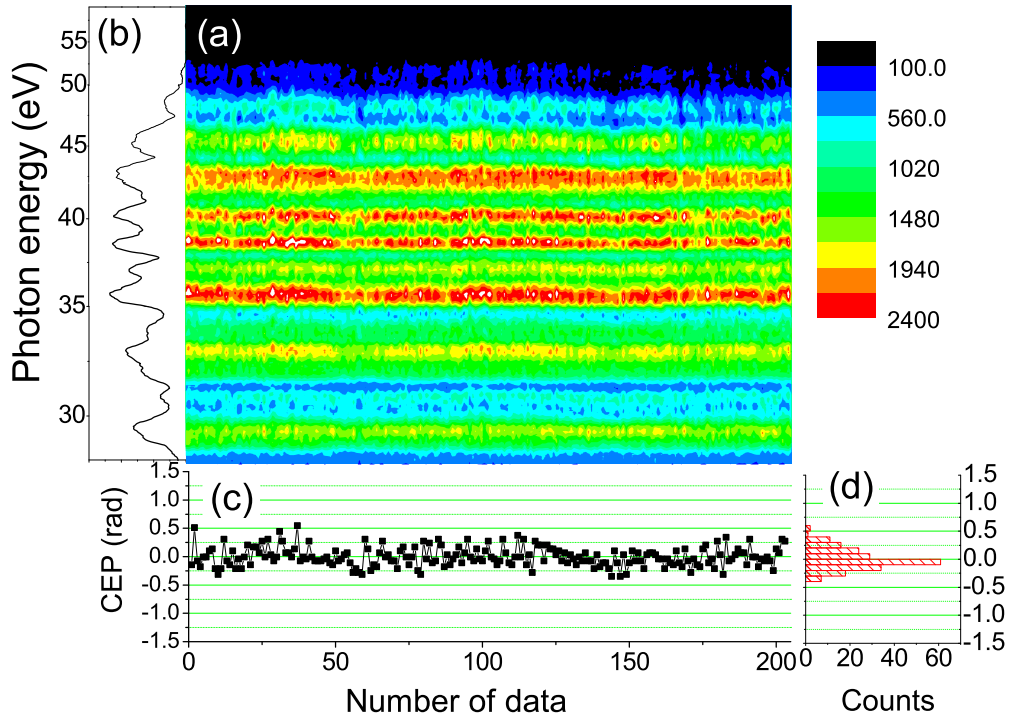


FIG. 7. (Color online) (a) The high-harmonic spectrum of CO_2 experimentally measured for individual laser shots. This provides a measure of the CEP stability of the laser system based on the HHG measurement rather than an optical measurement. The intensity is represented by color coding. (b) The high-harmonic spectrum corresponding to the first shot. (c) The value of CEP evaluated from the spectrum at each shot. (d) The statistics of the value of CEP.

spectral positions as a function of CEP can be related to the energy difference between two adjacent harmonics.

ACKNOWLEDGMENTS

The authors acknowledge the technical support of Bert Avery, and gratefully acknowledge the support from JSPS KAKENHI Grant No. 25247069, the National Research Council of Canada, and AFOSR (USA) Grant No. FA9550-13-1-0010.

APPENDIX

In this Appendix, we describe the details of calculation for Fig. 4. We calculate the Volkov phase [Eq. (10)] of three single attosecond emissions as a function of CEP. In Fig. 8, we illustrate the electric field of a driving laser pulse at CEP = 0 and the electron trajectories that are considered. Near each peak of the laser field, the electron is released into the ionization continuum by tunnel ionization. The electron recollision with the parent ion generates a single attosecond emission. This process occurs twice within one optical cycle in the driving laser pulse. Spectral interference between the different half-cycle emissions determines the positions of the peaks seen in the HHG spectra (see text). We consider three single attosecond emissions around the center of the electric field that are labeled as 1, 2, and 3.

First, we calculate the Volkov phase of each single emission as a function of CEP using Eq. (10). Figure 9 plots the calculated phases as a function of harmonic order at CEP of (a) 0 and (b) $-\pi/2$, respectively. In the cut-off range, two single

emissions contribute to the total harmonic spectra, while in the middle range three single emissions contribute to the total emission. As expected, the Volkov phase depends on the value of CEP.

We select two harmonic orders, i.e., 27th and 35th, and calculate the CEP dependence of the Volkov phases for each attosecond emission. Figure 10 plots the calculated Volkov phases for attosecond emissions labeled as 1, 2, and 3, i.e., θ_1 , θ_2 , and θ_3 , as a function of CEP for (a) 35th and (b) 27th harmonic order, respectively.

For 35th harmonic order, two attosecond emissions contribute to the harmonic spectrum except for the value around

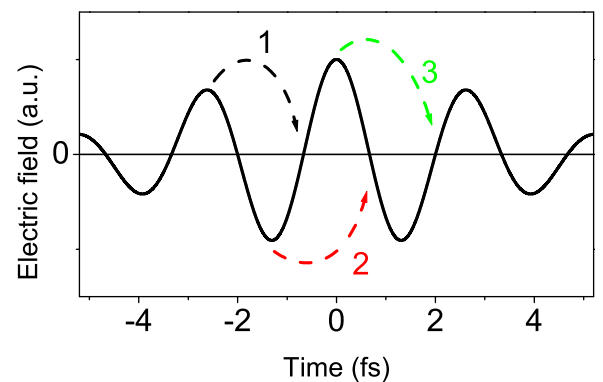


FIG. 8. (Color online) A schematic illustration of the electric field of a driving laser pulse at CEP = 0 and the electron trajectories that are considered.

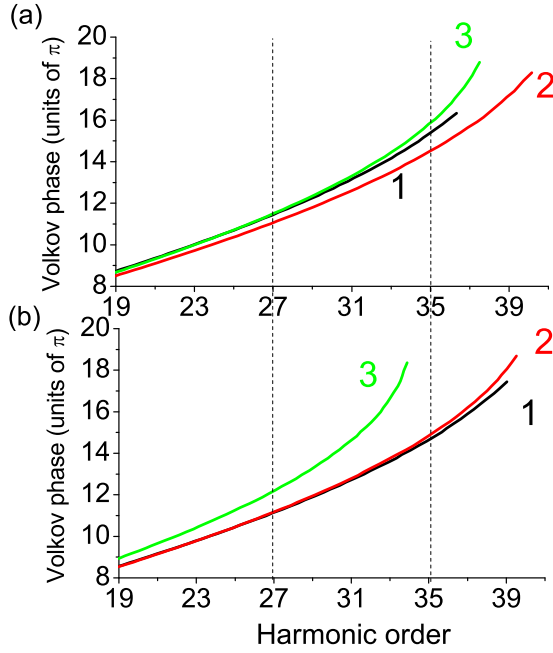


FIG. 9. (Color online) The calculated spectral phase (Volkov phase) of each single attosecond emission as a function of the harmonic number at a pulse duration of 7.0 fs and a CEP of (a) 0 and (b) $-\pi/2$, respectively. The numbers in the figures correspond to the half-cycles noted in Fig. 8 schematically.

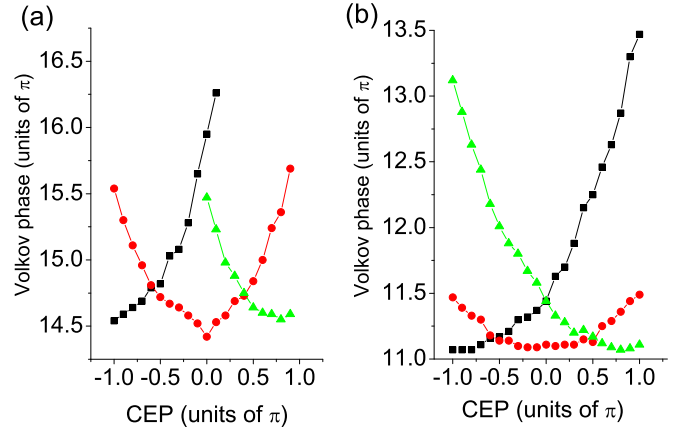


FIG. 10. (Color online) The calculated Volkov phases as a function of CEP for each single attosecond emission for (a) 35th and (b) 27th harmonic order, respectively. The square data points are the plots of the Volkov phase of the first emission (θ_1), the circles are the second (θ_2), and the triangles are the third emissions (θ_3), respectively.

CEP of 0, while for 27th harmonic order, three emissions contribute to the harmonic spectrum for all values of the CEP. For each harmonic order, we take the phase difference between the first and the second (θ_{12}), the second and the third (θ_{23}), and the first and the third (θ_{13}) as a function of CEP. The results are plotted in Fig. 4 in the main text.

- [1] F. Krausz and M. Y. Ivanov, *Rev. Mod. Phys.* **81**, 163 (2009).
- [2] P. B. Corkum and F. Krausz, *Nat. Phys.* **3**, 381 (2007).
- [3] A. Scrinzi, M. Y. Ivanov, R. Kienberger, and D. M. Villeneuve, *J. Phys. B* **39**, R1 (2006).
- [4] M. Drescher, M. Hentschel, R. Kienberger, M. Uiberacker, V. Yakovlev, A. Scrinzi, T. Westerwalbesloh, U. Kleineberg, and F. Krausz, *Nature (London)* **419**, 803 (2002).
- [5] J. Itatani, J. Levesque, D. Zeidler, H. Niikura, H. Pépin, J.-C. Kieffer, P. B. Corkum, and D. M. Villeneuve, *Nature (London)* **432**, 867 (2004).
- [6] O. Smirnova, Y. Mairesse, S. Patchkovskii, N. Dudovich, D. Villeneuve, P. Corkum, and M. Y. Ivanov, *Nature (London)* **460**, 972 (2009).
- [7] H. Niikura, H. J. Wörner, D. M. Villeneuve, and P. B. Corkum, *Phys. Rev. Lett.* **107**, 093004 (2011).
- [8] S. Haessler, J. Caillat, W. Boutu, C. Giovanetti-Teixeira, T. Ruchon, T. Auguste, Z. Diveki, P. Breger, A. Maquet, B. Carré, R. Taïeb, and P. Salières, *Nat. Phys.* **6**, 200 (2010).
- [9] H. J. Wörner, J. B. Bertrand, D. V. Kartashov, P. B. Corkum, and D. M. Villeneuve, *Nature (London)* **466**, 604 (2010).
- [10] W. Li, X. Zhou, R. Lock, S. Patchkovskii, A. Stolow, H. C. Kapteyn, and M. M. Murnane, *Science* **322**, 1207 (2008).
- [11] H. Niikura, D. M. Villeneuve, and P. B. Corkum, *Phys. Rev. Lett.* **94**, 083003 (2005).
- [12] P. B. Corkum, *Phys. Rev. Lett.* **71**, 1994 (1993).
- [13] Y. Mairesse, A. de Bohan, L. J. Frasinski, H. Merdji, L. C. Dinu, P. Monchicourt, P. Breger, M. Kovačev, R. Taïeb, B. Carré, H. G. Muller, P. Agostini, and P. Salières, *Science* **302**, 1540 (2003).
- [14] A. Baltuška, T. Udem, M. Uiberacker, M. Hentschel, E. Goulielmakis, C. Gohle, R. Holzwarth, V. S. Yakovlev, A. Scrinzi, T. W. Hänsch, and F. Krausz, *Nature (London)* **421**, 611 (2003).
- [15] S. Gilbertson, H. Mashiko, C. Li, S. D. Khan, M. M. Shakya, E. Moon, and Z. Chang, *Appl. Phys. Lett.* **92**, 071109 (2008).
- [16] C. A. Haworth, L. E. Chipperfield, J. S. Robinson, P. L. Knight, J. P. Marangos, and J. W. G. Tisch, *Nat. Phys.* **3**, 52 (2007).
- [17] C. Li, H. Mashiko, H. Wang, E. Moon, S. Gilbertson, and Z. Chang, *Appl. Phys. Lett.* **92**, 191114 (2008).
- [18] M. Lewenstein, P. Balcou, M. Y. Ivanov, A. L'Huillier, and P. B. Corkum, *Phys. Rev. A* **49**, 2117 (1994).
- [19] T. Brabec and F. Krausz, *Rev. Mod. Phys.* **72**, 545 (2000).
- [20] C. Iaconis and I. A. Walmsley, *Opt. Lett.* **23**, 792 (1998).
- [21] H. J. Wörner, H. Niikura, J. B. Bertrand, P. B. Corkum, and D. M. Villeneuve, *Phys. Rev. Lett.* **102**, 103901 (2009).
- [22] E. Goulielmakis, M. Schultze, M. Hofstetter, V. S. Yakovlev, J. Gagnon, M. Uiberacker, A. L. Aquila, E. M. Gullikson, D. T. Attwood, R. Kienberger, F. Krausz, and U. Kleineberg, *Science* **320**, 1614 (2008).
- [23] A. Fleischer and N. Moiseyev, *Phys. Rev. A* **74**, 053806 (2006).
- [24] V. S. Yakovlev, M. Ivanov, and F. Krausz, *Opt. Express* **15**, 15351 (2007).
- [25] G. Sansone, *Phys. Rev. A* **79**, 053410 (2009).
- [26] M. V. Frolov, N. L. Manakov, A. M. Popov, O. V. Tikhonova, E. A. Volkova, A. A. Silaev, N. V. Vvedenskii, and A. F. Starace, *Phys. Rev. A* **85**, 033416 (2012).
- [27] G. G. Paulus, F. Grasbon, H. Walther, P. Villaresi, M. Nisoli, S. Stagira, E. Priori, and S. De Silvestri, *Nature (London)* **414**, 182 (2001).
- [28] A. D. Shiner, C. Trallero-Herrero, N. Kajumba, B. E. Schmidt, J. B. Bertrand, K. T. Kim, H.-C. Bandulet, D. Comtois, J.-C. Kieffer, D. M. Rayner, P. B. Corkum, F. Legaré, and D. M. Villeneuve, *J. Mod. Opt.* **60**, 1458 (2013).